Mineralogical, Geochemical, and Isotopic Characteristics of the Ejecta From the 5 April 2003 Paroxysm at Stromboli, Italy: Inferences on the Preeruptive Magma Dynamics

Lorella Francalanci,[1] Antonella Bertagnini,[2] Nicole Métrich,[2,3] Alberto Renzulli,[4] Riccardo Vannucci,[5] Patrizia Landi,[2] Stefano Del Moro,[4] Michele Menna,[4] Chiara Maria Petrone,[1] and Isabella Nardini[1]

The 5 April 2003 explosive eruption at Stromboli emplaced typical basaltic scoria, pumice, and lithic blocks. This paper reports a detailed set of mineralogical, geochemical, and isotopic data on the juvenile ejecta and fresh subvolcanic blocks, including micro-Sr isotope analyses and major and dissolved volatile element contents in olivine-hosted melt inclusions. The juvenile ejecta have compositions similar to those of their analogs from previous paroxysms; the 2003 pumice, however, does not contain stable high-MgO olivine, usually typical of large-scale paroxysms and has lower compatible element contents. Texture, composition, and Sr isotope disequilibrium of crystals in pumice indicate that most of them are inherited from the shallow crystal-rich magma and/or crystal mush. The most primitive magma is recorded as rare melt inclusion in olivine $Fo_{85–86}$. It has a typical S/Cl (1.1) and a total volatile content of 3.1 wt % from which the total fluid pressure was evaluated ≥240 MPa. Hence, moderate pressure conditions can be envisaged for the mechanism triggering the April 2003 paroxysm. The subvolcanic blocks are shoshonitic basalts with 45–50 vol % of phenocrysts (plagioclase + clinopyroxene + olivine). The late-stage crystallization of the crystal-rich magma lead to the formation of Na-sanidine with plagioclase $An_{60–25}$ + olivine $Fo_{68–49}$ + Ti-magnetite ± apatite ± phlogopite ± ilmenite assemblage. Mineralogy, chemistry,

[1] Dipartimento di Scienze della Terra, Università degli Studi di Firenze, Firenze, Italy.

[2] Istituto Nazionale di Geofisica e Vulcanologia, Sezione di Pisa, Italy.

[3] Laboratoire Pierre Süe, CEA-CNRS, CE-Saclay, Gif-sur-Yvette, France.

[4] Istituto di Scienze della Terra, Università degli Studi di Urbino, Campus Scientifico, Urbino, Italy.

[5] Dipartimento di Scienze della Terra, Università di Pavia, e CNR-IGG, Pavia, Italy.

TITLE
Geophysical Monograph Series XXX
XXXXXXXXXXXXXXXXXXXXXXXXXXX
10.1029/XXXGMXX

and Sr–Nd isotopic signatures of the subvolcanic blocks indicate they represent the slowly cooled equivalents of batches of crystal-rich basaltic magma stored in the uppermost subvolcanic feeding system during short breaks in the summit crater activity ~~of the last few years~~.

1. INTRODUCTION

The paroxysm of 5 April 2003 has been the most violent event of the past 50 years. The eruption occurred while lava emission was in progress from lateral vents and consisted of an 8-min-long explosive sequence. The most energetic explosion launched meter-sized ballistic blocks that fell on the volcano flanks and on the village of Ginostra, about 2 km far from the vent. A vertical gas/pyroclastic jet rose above the craters, feeding a convective plume that reached a height of up to 4 km. A fallout deposit of coarse pyroclasts (bombs and blocks) with subordinate amount of fine ash blanketed the upper part of the cone, while a shower of light pumice fell on the southern slopes of the volcano, down to the sea.

The juvenile clasts mainly consisted of light-colored, crystal-poor pumice variably mingled with dark-colored, crystal-rich scoria, which was formed by the same magma feeding the lava flows. Lithic fragments were very abundant and consisted of cognate, angular holocrystalline igneous rocks and variably altered volcanic scoria and lava [*Rosi et al.*, 2006; *Pistolesi et al.*, this volume].

Pumice and scoria bombs (hereafter pumice and scoria) and the most common and fresh lithics, mostly represented by subvolcanic rocks, were sampled for mineralogical, geochemical, and isotopic studies.

Bulk samples, matrix glasses, and minerals were analyzed for major and trace elements in different laboratories using a variety of bulk and in situ methods. Major and volatile elements were also determined in olivine-hosted silicate melt inclusions (MI) from pumices. Sr and Nd isotope data were performed on bulk samples and glassy groundmasses, whereas micro-Sr isotope ratios were determined on plagioclase and clinopyroxene of pumice and scoria by the microdrilling technique [I. Nardini, L. Francalanci, D. G. Chertkoff, M. Tiepolo, R. Avanzinelli, J. P. Davidson, and R. Vannucci, *In-situ* chemical and isotopic analyses in the Stromboli products of the 2002–2003 eruptive crisis: Micro-scale variations recording macro-scale processes, submitted to *Contributions to Mineralogy and Petrology*, 2008, hereinafter referred to as Nardini et al., submitted manuscript, 2008]. Separation procedures were applied to obtain pumice and scoria fractions from the mingled ejecta for whole-rock analyses. About 90 clinopyroxene and 600 olivine crystals were carefully handpicked from the 1- to 0.25-mm grain-size pumice fraction for petrographic and MI analyses [*Métrich et al.*, 2005].

2. JUVENILE EJECTA

2.1. Petrography and Major and Trace Element Composition of Minerals

The 5 April scoria samples have petrographic and mineralogical characteristics similar to those of the scoria erupted by the normal Strombolian activity; they have highly porphyritic texture (~45–55 vol % of phenocrysts and microphenocrysts) and mainly hyaline to cryptocrystalline groundmass. Olivine (≈5 vol %), up to 3 mm in size, clinopyroxene (≈15 vol %), up to 0.5 cm in size, and plagioclase (≈35 vol %), up to 2 mm in size represent the phenocrysts, whereas microphenocrysts are mostly represented by plagioclase and rare olivine. The prevailing composition of olivine from scoria is forsterite (Fo) 70–73%, with small normal or reverse zoning. Clinopyroxene shows oscillatory zoning, from Mg # [mole Mg/(Mg + Fe)] 0.89 to 0.75. Resorbed clinopyroxene cores are often present. Plagioclase from scoria displays a large spectrum in anorthite (An) contents (65–86%), with outer rims generally showing the lowest An values. The largest plagioclase crystals usually have resorbed cores with concentric compositional and textural zoning.

In situ trace element contents were analyzed by laser ablation microprobe inductively coupled plasma (ICP)–mass spectrometry (MS) (see *Tiepolo et al.* [2003] for instrumentation and analytical procedures) on some plagioclase and clinopyroxene crystals (Figures 1a and 1b). Chondrite-normalized [*Anders and Grevesse*, 1989] patterns indicate positive anomalies for Ba, Sr, and Eu in plagioclase, with no correlation between An and trace element contents. Only Th and Ta contents seem to be higher in the rim with lower An component than the outer core (Figure 1a). Chondrite-normalized trace element values of clinopyroxene are in the range between 0.1 and 100. For zones with Mg # <0.82, heavy rare earth element (REE_N) are around 10, and middle and light REE_N and Ni_N are >10. Zones with Mg # >0.82 have lower Hf_N, Zr_N, Y_N, and REE_N. The light REE have convex upward patterns, similar in both Mg-rich and Mg-poor zones. The latter are characterized by small negative Eu

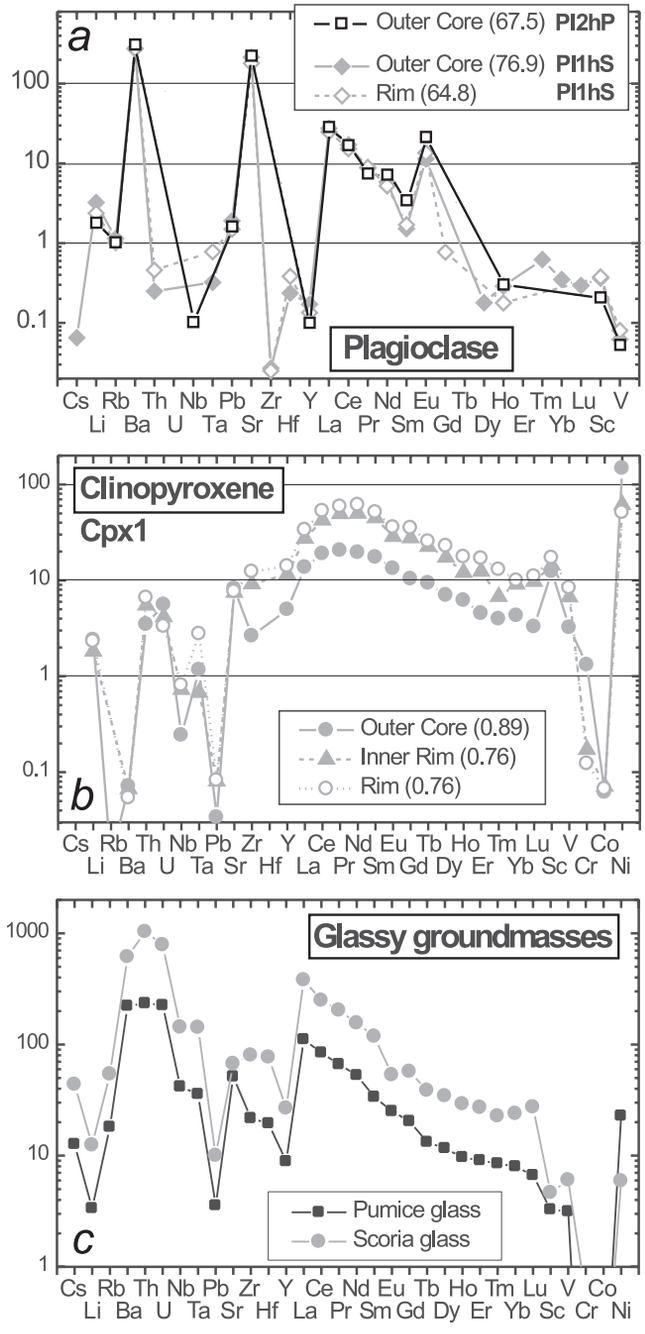

Figure 1. Chondrite-normalized [*Anders and Grevesse*, 1989] trace element patterns for (a) plagioclase, (b) clinopyroxene, and (c) matrix glasses of scoria (gray) and pumice (black). Trace elements were determined by laser ablation–ICP–MS at CNR-IGG, Pavia. An % for plagioclase and Mg # [mole Mg/(Mg + Fe)] for clinopyroxene of the analyzed zones are also given in the legends. Pl1hS, Pl2hP, and Cpx1 are referred to the name of crystals drilled for micro-Sr isotope ratios and reported in Figure 5. Element ordering: rare earth elements have been reported separately from the other elements, which are in order of increasing compatibility into a basaltic mineral assemblage.

anomalies (Eu/Eu* around 0.8), possibly suggesting lower oxygen fugacity of the host magma with respect to the crystallizing conditions of the Mg-rich zones (Figure 1b).

The 5 April pumice samples carry up to 15–20 vol % of crystals settled in a glassy groundmass. As previously verified in other paroxysmal events, most of them (the dominant proportions of minerals in grain sizes >1 mm) are "xenocrysts" of plagioclase, clinopyroxene, and olivine-entrained and inherited from the shallow crystal-rich magma body [*Métrich et al.*, 2001; *Francalanci et al.*, 2004b].

In grain sizes <1 mm, olivine shows a broad compositional and textural heterogeneity. The most abundant olivine crystals are represented by (1) euhedral crystals with homogeneous Fe-rich cores ($Fo_{66–71}$), surrounded by a heterogeneous mottled zone of variable width, and a thin Mg-richer outer rim ($Fo_{82–86}$; Figure 2a); (2) heterogeneous patchy-zoned euhedral crystals ($Fo_{75–83}$) surrounded by outer Mg-rich rims ($Fo_{82–87}$). The chemical variability, systematic reverse zoning, and resorption textures indicate that these olivine crystals (1 and 2) represent different stages of reaction with a more primitive melt than their host liquid. Crystals with Fe-rich cores ($Fo_{66–71}$) are interpreted as drained-back from the shallow magmatic body and/or from the most evolved parts of the upper plumbing system, as already observed in the Stromboli pumice [*Métrich et al.*, 2001; *Francalanci et al.*, 2004b, 2005]. Variable growth of reaction zones indicates different times of reaction and, thus, residence of recycled crystals in pumicelike melts. The patchy-zoned olivine ($Fo_{75–83}$) is indicative of unstable conditions during resorption–crystallization processes, a feature previously observed [see *Bertagnini et al.*, 2003, for discussion]. Minor anhedral crystals ($Fo_{79–82}$) with lobate margins ($Fo_{84–85}$) are also present (Figure 2b). A very small fraction (~1%) of the handpicked olivine is constituted by euhedral microphenocrysts (nearly 0.5 mm in size) with a restricted compositional range ($Fo_{85–87}$; Figure 2c). They are either slightly normally or reversely zoned [*Métrich et al.*, 2005].

Clinopyroxene crystals show similar characteristics. Only a few homogenous $Wo_{45–48}$–$Fs_{7–8}$ microphenocrysts are present, while most of the studied crystals are reversely zoned with resorbed cores and variable (50–500 μm) rims of composition $Wo_{44–48}$–$Fs_{7–10}$. Besides, the core chemistry is that expected for clinopyroxene in equilibrium with the shallow-sited magma ($Wo_{43–46}$–$Fs_{12–16}$), more Fe-rich and less calcic compositions are frequent ($Wo_{38–41}$, $Fs_{17–19}$) [*Métrich et al.*, 2005].

Most of the plagioclase crystals have compositional range ($An_{64–86}$), zoning, and texture similar to those shown by their analogs from scoria, indicating their origin from the shallow crystal-rich magma reservoir. Only rare plagioclase microphenocrysts have high An contents (from core to outer rim, 85%–89%), representing the minerals in equilibrium with

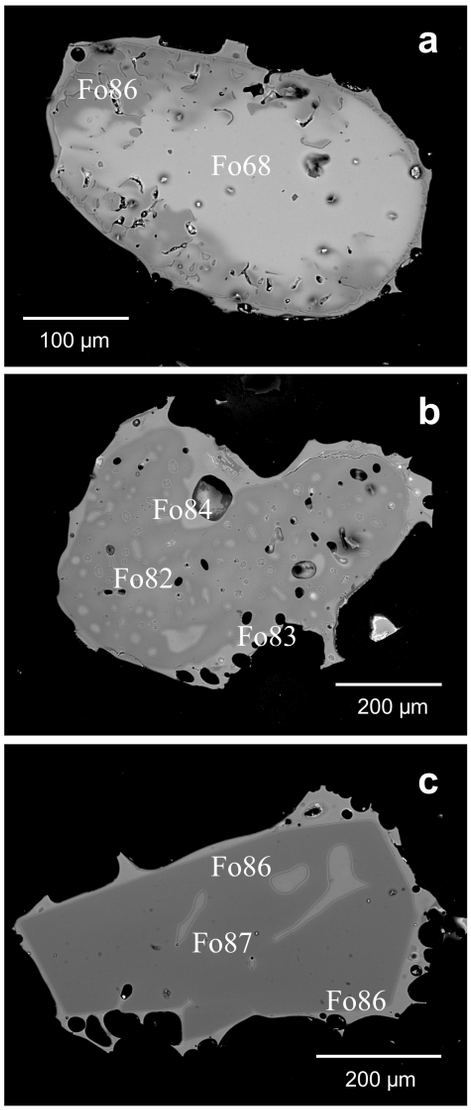

Figure 2. Backscattered electron microphotographs of olivine from pumice of the 5 April 2003 paroxysm. (a) Euhedral crystals with homogeneous Fe-rich cores and more forsteritic rims. (b) Anhedral olivine with a large amount of MIs, open gulfs (embayments), and bubbles, testifying to the ultimate stage of crystallization. (c) Primitive euhedral olivine with isolated MI.

the pumice magma, crystallized for water lost at the ultimate stage of their transfer to the surface. These high An contents were also found in pumice from the previous small-scale paroxysms that occurred between 1996 and 2000 [*Francalanci et al.*, 2004b].

A plagioclase outer core from pumice has a chondrite-normalized trace element pattern similar to that of plagioclase from scoria, including the amplitude of Ba-, Sr-, and Eu-positive anomalies (Figure 1a). The low An content (67%) of this plagioclase is also indicative of its origin from the crystal-rich magma.

2.2. Major and Trace Element Compositions of Whole Rocks and Matrix Glasses

The bulk pumices emitted on 5 April 2003 plot on the boundary line between shoshonitic and high-K basalts of the K_2O versus silica classification diagram, similarly to the previously erupted pumices (Table 1). They belong to the typical domain of the historical to present-day pumices with respect to their major and trace element compositions, except for their slightly lower Cr contents (28–40 ppm with respect to 45–55 ppm of previous pumice; data ranges based on different analytical methods).

Because of the diffuse mingling between scoria and pumice, bulk-rock chemical analyses of the two lithotypes could not be completely representative of the two end members, despite our efforts in separating the two fractions. Bulk-rock composition of 5 April scoria, however, seems to strictly resemble that of the previous crystal-rich magmas (Table 1). Furthermore, major and trace element contents of the scoria glassy groundmasses closely match those of the earlier crystal-rich products, with K_2O 4.0–4.7 wt % and Al_2O_3 15–16 wt % (Table 2; Figure 3). Q1

The matrix glasses of 5 April 2003 pumice show higher MgO, CaO, and Al_2O_3 (17.4–18.2 wt %) and lower FeO, TiO_2, K_2O (1.9–2.2 wt %), Na_2O, P_2O_5, and incompatible trace element contents than the glassy groundmasses of the coeval scoria (Table 2, Figures 1c and 3). These compositional variations are those typically observed between scoria and pumice matrix glasses from the recent Strombolian activity. As already observed for whole rocks, glassy groundmass of 5 April 2003 pumice is similar in composition to the previous pumices, except for slightly lower Cr and Sc contents of the former [*Francalanci et al.*, 2004a].

Chondrite-normalized trace element patterns for both pumice and scoria show large overall REE-negative fractionation, positive Th and U, and negative high field strength elements spikes, as usually observed in Stromboli K-enriched series [*Francalanci et al.*, 1989; *Tommasini et al.*, 2007]. Noticeably, higher abundance levels, coupled with negative Sr and Eu anomaly, characterize scoria matrix glasses, in agreement with the crystallization of a plagioclase-bearing mineral assemblage in the crystal-rich magma (Figure 1c).

2.3. Sr, Nd, and Micro-Sr Isotope Data in Pumice and Scoria

Whole-rock and matrix glass of 5 April 2003 pumice show comparable $^{87}Sr/^{86}Sr$ values, i.e., ~0.70611. This value falls

Table 1. Major and Trace Element Analyses of Representative Whole Rock Samples of Pumice and Scoria

Sample	STR[a] 050403hP pumice	STR[b] 050403hP pumice	STR[a] 050403k pumice	STR[b] 050403k pumice	ST[c] 317 pumice	ST[c] 320 pumice	ST[c] 333 pumice	ST[c] 300 pumice	ST[c] 325a scoria	ST[c] 325b scoria
SiO_2, wt %	49.23	49.44	49.77	49.34	48.38	48.63	48.99	49.51	49.22	49.31
TiO_2	1.01	0.91	0.98	0.91	0.90	0.91	0.91	0.92	0.91	0.92
Al_2O_3	17.06	17.60	16.85	17.32	17.21	17.45	17.14	17.06	17.33	16.93
Fe_2O_3	3.27	8.81	3.03	8.71	8.95	8.84	8.80	8.76	8.75	8.74
FeO	5.84	–	5.76	–	–	–	–	–	–	–
MnO	0.17	0.16	0.17	0.16	0.16	0.16	0.16	0.15	0.16	0.16
MgO	6.70	6.07	6.86	5.98	6.64	6.36	6.33	6.36	6.24	6.19
CaO	11.72	11.56	11.67	11.65	12.01	11.92	11.80	11.76	11.54	11.24
Na_2O	2.41	2.45	2.47	2.48	2.40	2.43	2.44	2.43	2.52	2.55
K_2O	1.84	1.89	1.77	1.77	1.84	1.87	1.89	1.85	2.08	2.15
P_2O_5	0.37	0.55	0.37	0.53	0.59	0.61	0.56	0.54	0.61	0.57
LOI	0.39	0.44	0.30	0.74	0.78	–0.02	0.33	0.43	0.22	0.19
CaO/Al_2O_3	0.69	0.66	0.69	0.67	0.70	0.68	0.69	0.69	0.67	0.66
K_2O/Na_2O	0.76	0.77	0.72	0.72	0.77	0.77	0.77	0.76	0.83	0.84
V, ppm	279	254	273	251	286	278	280	279	272	282
Cr	36	29	31	28	40	36	39	35	47	52
Co	37	31.0	34	34.6	35	34	34	34	33	34
Ni	–	34	–	34	44	41	41	41	40	41
Sc	–	29	–	29	–	–	–	–	–	–
Cu	118	132	112	126	–	–	–	–	–	–
Zn	72	62	71	64	–	–	–	–	–	–
Cs	–	3.5	–	3.7	3.4	3.5	3.7	3.6	4.2	4.5
Rb	51	56	52	59	57	58	60	59	67	71
Sr	787	722	778	716	715	730	729	740	731	753
Y	25	24.7	25	27.1	25	25	26	26	26	27
Zr	144	127	132	123	145	146	149	149	159	167
Nb	19	17.6	18	18.9	16	16	16	16	18	19
Mo					1.18	1.16	1.21	1.27	1.44	1.52
Ba	857	826	825	801	841	860	874	878	940	984
La	42	37.9	42	41.1	40	41	42	42	45	47
Ce	99	84.2	85	91.1	82	84	85	86	91	94
Pr	–	10.1	–	11.1	9.8	10.03	10.17	10.25	10.77	11.06
Nd	44	38.7	43	42.6	39	40	40	41	42	43
Sm	–	7.65	–	8.26	7.8	7.9	8.0	8.0	8.4	8.6
Eu	–	2.15	–	2.40	2.1	2.2	2.2	2.2	2.2	2.3
Gd	–	6.47	–	7.03	6.5	6.6	6.5	6.7	6.8	7.0
Tb	–	0.97	–	1.07	0.90	0.91	0.92	0.94	0.95	0.96
Dy	–	4.94	–	5.36	4.81	4.87	4.96	5.01	5.03	5.18
Ho	–	0.90	–	1.01	0.89	0.89	0.90	0.92	0.93	0.93
Er	–	2.47	–	2.71	2.33	2.37	2.43	2.43	2.45	2.51
Tm	–	0.329	–	0.361	0.34	0.35	0.35	0.35	0.35	0.37
Yb	–	2.27	–	2.49	2.18	2.21	2.24	2.27	2.32	2.39
Lu	–	0.338	–	0.375	0.34	0.34	0.35	0.35	0.36	0.36
Hf	–	3.3	–	3.5	3.3	3.4	3.4	3.4	3.6	3.8
Ta	–	1.3	–	1.4	1.02	1.05	1.05	1.09	1.19	1.23
Pb	19	15	20	17	14	16	18	17	17	17
Th	–	12.1	–	13.0	11.4	12.0	12.4	12.3	14.2	14.9
U	–	2.90	–	3.20	2.94	3.08	3.15	3.14	3.67	3.81

[a] All elements were analyzed by XRF at the Department of Earth Science of Florence, Italy.

[b] Major elements were analyzed by XRF and trace elements by ICP–atomic emission spectrometry + ICP–MS at the SGS Minerals Services of Toronto, Ontario, Canada.

[c] All elements were analyzed at Service d'Analyse des Roches et des Minéraux, CRPG, Nancy, France.

Table 2. Representative Compositions of MIs in Olivine From 5 April 2003 Pumice and of Matrix Glass in Pumice and Scoria

Sample	ST304	ST300	ST300	ST300	ST300	ST304	ST304	ST304	ST306p	ST304s
Inclusion[a]	3a (3)	34a (4)	34b (2)	33a (1)	33d (1)	19a (4)	22-2 (1)	22-2 (1)	mg (5)	mg (5)
SiO_2, wt%	47.77	47.93	47.55	47.45	47.15	47.23	47.34	49.07	48.98	52.36
TiO_2	0.91	0.87	0.87	0.91	0.96	0.88	0.91	1.14	0.98	1.59
Al_2O_3	16.83	16.57	16.59	16.60	17.55	16.93	17.16	17.37	17.63	15.52
FeO total	7.73	8.49	8.21	8.49	7.75	8.12	7.96	8.12	8.13	10.05
MnO	0.13	0.12	0.17	0.13	0.06	0.13	0.22	0.30	0.19	0.20
MgO	6.42	6.75	6.69	6.04	5.85	6.47	6.18	6.20	5.97	3.22
CaO	12.81	11.78	11.55	11.73	12.08	12.06	11.51	11.52	11.57	7.11
Na_2O	2.03	2.41	2.31	2.17	2.41	2.15	2.61	2.45	2.53	3.40
K_2O	1.41	1.65	1.68	1.48	1.66	1.51	1.94	1.90	1.92	4.25
P_2O_5	0.66	0.56	0.57	0.56	0.49	0.58	0.60	0.60	0.61	1.19
S	0.157	0.128	0.140	0.148	0.119	0.152	0.097	0.060	0.022	0.009
Cl	0.154	0.155	0.151	0.133	0.128	0.191	0.139	0.144	0.114	0.118
H_2O	2.5	2.0	2.1	N.D.	N.D.	N.D.	0.8	0.5	N.D.	
CO_2, ppm	1673	1428	1603	2123	1301	1094	368	N.D.	N.D.	
Total	99.71	99.58	98.73	96.05	96.35	96.52	97.46	99.38	98.65	99.02
Olivine, Fo mol %	86.4	85.8	86.1	83.8	85.0	85.7	84.6	84.6		
% PEC	0.04	0.06	0.07	0.10	0.03	0.04	0.03	0.00		
CaO/Al_2O_3	0.76	0.71	0.69	0.70	0.69	0.71	0.67	0.66	0.66	0.46
S/Cl	1.02	0.82	0.92	1.12	0.93	0.80	0.69	0.41	0.20	0.08
K_2O/Na_2O	0.69	0.69	0.73	0.68	0.69	0.70	0.74	0.77	0.76	1.25
Pressure, MPa[b] (4)	299	244	270				61			

Major and volatile elements are corrected for olivine postentrapment crystallization (% PEC). Fo mol% = [100 × Mg/(Fe + Mg)].
[a] In parentheses is the number of analyzed points per inclusion and matrix glass (mg). p, Pumice; s, scoria; N.D., not determined.
[b] Pressure calculated using VolatileCalc [*Newman and Lowernstern*, 2002]. Analytical techniques are from *Métrich et al.* [2005].

in the isotopic range of the previously erupted pumice since 1996 (Table 3, Figure 4). A higher $^{87}Sr/^{86}Sr$ value (~0.70615) is shown by the glassy groundmass of scoria. This value well compares with those for 2002–2003 lavas erupted before and a few days after (14 April 2003) the 5 April paroxysm (Table 3).

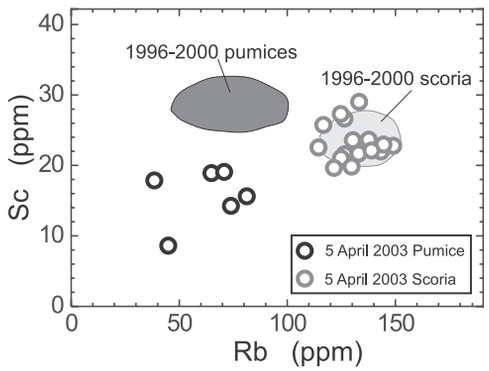

Figure 3. Rb versus Sc diagram for the matrix glass compositions of scoria and pumice from the 5 April 2003 paroxysm. Compositional fields of the matrix glasses of scoria–pumice pairs from the 1996–2000 paroxysms are also reported for comparison. All data are analyzed by LAM at the University of Pavia.

Nd isotope ratios of bulk rock and groundmass of 5 April 2003 pumice and scoria are around 0.51257, akin to the values measured in 1996 and 1999 pumices [*Francalanci et al.*, 2004b, unpublished data]. $^{143}Nd/^{144}Nd$ of scoria groundmass is about 0.512556 (Table 3), a value well in the range of 1996–2000 scoria [*Landi et al.*, this volume; Nardini et al., submitted manuscript, 2008]. Accordingly, Nd isotope ratios between 5 April 2003 scoria and pumice are less variable than Sr isotope ratios, and this makes the Nd isotopes less relevant for understanding the magma dynamics at Stromboli.

Micro-Sr isotope data have been performed on core–rim traverses of plagioclase and clinopyroxene by microdrilling technique. The analyses were generally focused on crystals showing marked zoning. The different crystal zones were sampled by a Micromill instrument, and Sr isotope ratios were analyzed using standard chemical separation techniques (at the University of Durham, UK) and a thermal ionization mass spectrometer (at the University of Flor-

Table 3. Representative Sr and Nd Isotope Ratios of Ejecta From the 5 April 2003 Paroxysm

Sample	Ejecta	$^{87}Sr/^{86}Sr$	2 SD	$^{143}Nd/^{144}Nd$	2 SD
STR050403k[a]	Pumice	0.706098	0.000007	0.512567	0.000004
STR050403hP[a]	Pumice	0.706111	0.000007	0.512574	0.000004
STR050403h[a]	Pumice gdm	0.706116	0.000005	0.512572	0.000004
STR050403i[a]	Scoria gdm	0.706150	0.000007	0.512558	0.000004
STR050403r	Lithic	0.706159	0.000006	0.512563	0.000005
STR050403s	Lithic	0.706160	0.000006	0.512563	0.000004
STR050403t	Lithic	0.706171	0.000008	–	–
STR050403y	Lithic	0.706152	0.000006	–	–
		Micro-Sr analyses			
STR050403f[a]	Scoria	0.706401	0.000011	Plagioclase 3 core	
STR050403f[a]	Scoria	0.706183	0.000009	Plagioclase 3 rim	
STR050403h[a]	Scoria	0.706146	0.000008	Olivine crystal	
STR050403hP[a]	Pumice	0.706234	0.000015	Plagioclase 2 middle	
STR050403hP[a]	Pumice	0.706290	0.000008	Plagioclase 2 rim	

[a] Data from Nardini et al. [submitted manuscript, 2008]. Analyses were performed by thermal infrared multispectral scanning at the Department of Earth Sciences of Florence according to *Avanzinelli et al.* [2005] and for micro-Sr analyses, to Nardini et al. [submitted manuscript, 2008]. Replicate measurements of NBS 987 [0.710249; *Thirlwall*, 1991] and La Jolla [0.511856; *Thirlwall*, 1991] standards during the period of these analyses gave mean values of $^{87}Sr/^{86}Sr = 0.710250 \pm 0.000012$ (2 SD, $n = 78$) and $^{143}Nd/^{144}Nd = 0.511847 \pm 0.000007$ (2 SD, $n = 21$). gdm, groundmass.

ence, Italy; specific procedures according to *Charlier et al.* [2006]). Pronounced isotopic disequilibria were found in most of the crystals analyzed both in pumice and scoria (Figure 5). The cores and intermediate zones of minerals generally have higher Sr isotope ratios than outer rim and groundmasses, signifying they were crystallized from more Sr-radiogenic magmas than the host melt. Only the internal zone of one clinopyroxene grain, which included a large Mg-rich (Mg # >0.82) band, has given quite low Sr isotope ratios. On the other hand, $^{87}Sr/^{86}Sr$ values comparable with those of groundmasses were observed in two outer rims of coexisting plagioclase and clinopyroxene from scoria; this suggests that isotopic equilibrium was achieved during the final magma crystallization stages (Figure 5) [Nardini et al., submitted manuscript, 2008].

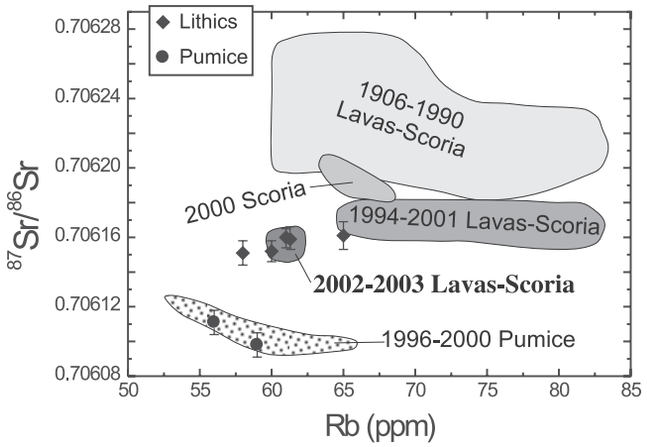

Figure 4. $^{87}Sr/^{86}Sr$ versus Rb for 5 April 2003 pumice and subvolcanic lithics, with compositional fields of previously erupted products since 1900 activity. The variation field of the nearly coeval 2002–2003 lavas and scoria is also separately reported. It is worth noting that the youngest products of the previous activity generally plot at lower Sr isotope ratios. Data for fields from *Francalanci et al.* [1999, 2004b, 2005], *Landi et al.* [2006, this volume], and Nardini et al. [submitted manuscript, 2008].

Sr isotopic disequilibria were already reported for the shallow crystal-rich magmatic system of the present-day Stromboli, at least since 1984. It has been suggested that the deeper and crystal-poor magma periodically recharging the shallow crystal-rich reservoir passes through an old cumulus and more Sr-radiogenic crystal-mush reservoir. Minerals from the old and more Sr-radiogenic reservoir are thus sampled by the uprising crystal-poor magma and transported into the shallower reservoir where mixing and crystallization processes led to the development around crystals of outer rims in isotopic equilibrium with the residual liquids [*Francalanci et al.*, 2005]. The in situ isotope data reported on 5 April 2003 juvenile ejecta suggest that crystal recycling still persist, and the plumbing system behaves as in the previous two decades at least.

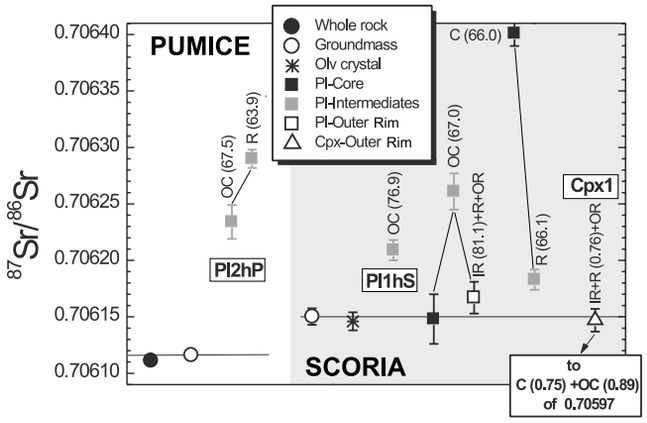

Figure 5. Micro-Sr isotope ratios for core–rim traverses in clinopyroxene and plagioclase of 5 April 2003 pumice and scoria. Isotope data on a separated olivine crystal, on whole rocks, and groundmasses are also reported. The white and gray areas of the diagram indicate the pumice and scoria portions, respectively. Micromillings of the different crystal zones and the Sr chemical separation have been performed at the University of Durham, whereas the Sr isotope ratios were measured at the University of Florence; Sr and Nd isotope analyses of bulk rocks and groundmasses have been entirely carried out at the University of Florence (see *Avanzinelli et al.* [2005] for instrumentation and methods). Legend of the core–rim traverse of minerals: full black symbols, crystal cores; full gray symbols, intermediate zones of crystals; open black symbols, prevalent outer rims; C, core; OC, outer core; IR, inner rim; R, rim; OR, outer rim. Pl2hP, Pl1hS, and Cpx1 refer to crystals also analyzed for trace elements by LAM and reported in Figures 1a and 1b. Modified after Nardini et al. [submitted manuscript, 2008].

2.4. Major and Volatile Element Data of Olivine-Hosted Melt Inclusions in Pumice

Major and volatile element compositions of MI, textures, and compositions of their host olivine were systematically studied in seven pumice samples both from distal and proximal fallout deposits [*Métrich et al.*, 2005].

Q2 Brownish MI in Fe-rich olivine ($\leq Fo_{71}$) are compositionally equivalent ($CaO/Al_2O_3 < 0.5$, $K_2O > 3.5$ wt %) to the glassy groundmass of the crystal-rich magma residing at shallow level. Melt (inclusions, embayments) trapped in large quantity in patchy-zoned olivine ($Fo_{75–83}$) systematically show variable enrichment in their Fe and Ca content and depletion in alkalis, in agreement with successive dissolution–crystallization events, as reported by *Bertagnini et al.* [this volume]. Instead, the chemical magma variability is recorded in MI and embayments (gulfs) that are entrapped in $Fo_{87–79}$ olivine, and it is accompanied by a change in size and morphology of inclusions and by textural evolution of their host olivine. Euhedral microphenocrysts ($Fo_{83–87}$) host HK-basaltic MI that are more primitive than the bulk pumice ($CaO/Al_2O_3 \leq 0.70$; Figure 6). In contrast, anhedral crystals ($Fo_{79–82}$) with lobate margins ($Fo_{84–85}$) trapped a large amount of melt and bubbles (Figure 2b). Their MI and embayments (gulfs) chemically resemble the matrix, and these crystals probably represent the ultimate stage of crystallization, just prior to eruption. The overall evolution tracked by the olivine-hosted MI would be explained by the combined effect of crystal fractionation and mixing. Upon ascent, mixing would occur at least at local scale, between HK-basaltic magmas that slightly differed in their evolution degrees and possibly in their initial K_2O content (on average, K_2O/Na_2O ratio varies from 0.67 to 0.76) [*Métrich et al.*, 2005].

As a whole, the dissolved contents of H_2O (from 2.5 to 0.5 wt %; Figure 7a) and CO_2 (from 0.21 to 0.037 wt %; Figure 3b) widely vary. MI and embayments in anhedral olivine ($Fo_{79–82}$) track syn-eruptive degassing of water and decrease in the S/Cl ratio ($2.0 > H_2O \geq 0.8$; $0.8 > S/Cl \geq 0.6$; Figure 7a). MI (CaO/Al_2O_3~0.69–0.70) in single olivine ($Fo_{83–86}$) show the broadest extents of variation in CO_2 (0.21–0.11 wt %; Figure 7b) and lowering in their S/Cl ratio (from 1.12 to 0.8). Since immiscible sulfide globule has not

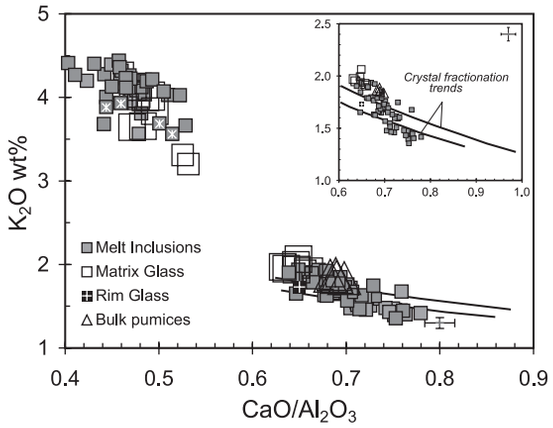

Figure 6. Variation of K_2O versus CaO/Al_2O_3 in olivine-hosted MI, matrix glasses and bulk rocks from the 5 April 2003 eruption [squares with an asterisk correspond to evolved MI in olivines ($Fo_{66–71}$) with reaction zones]. Trends of fractional crystallization are calculated with MELTS [*Ghiorso and Sack*, 1995] for parental melts containing 1.45 and 1.35 wt % K_2O, respectively, between 300 and 250 MPa and 1180°–1130°C. The inset shows the enlargement of the chemical variation of MI in olivine $Fo_{79–87}$. Modified from *Métrich et al.* [2005].

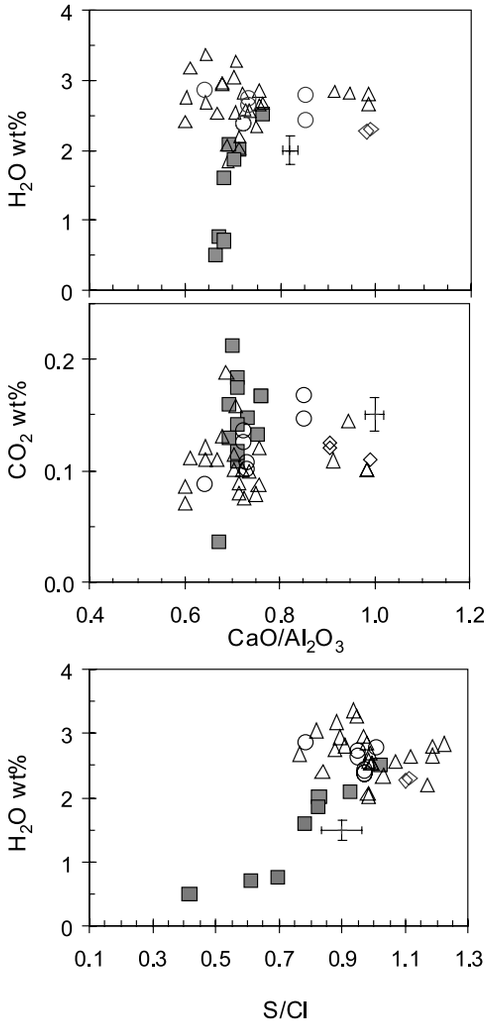

Figure 7. Volatile variability in MI hosted in olivine crystals from 5 April 2003 pumice (filled symbols) and from pumices emitted (triangle, samples ST81; diamond, ST79, 207; circle, ST82) during the most violent historical paroxysms (empty symbols) [*Métrich et al.*, 2001; *Bertagnini et al.*, 2003, unpublished data]. Modified from *Métrich et al.* [2005].

been observed, the combined decrease in S/Cl ratio and CO_2 content has been related to degassing and melt entrapment during decompression, in agreement with high and variable proportions of melt and bubble entrapped in this olivine. Kinetic effects, however, resulting in local enrichment in CO_2 dissolved in melt cannot be totally excluded. It is worth noting the water richness (up to 2.5 wt %) of the most primitive inclusions in $Fo_{85–87}$ and their high S/Cl ratio (1.1), typical of HK-basaltic magma at Stromboli [*Métrich et al.*, 2001].

The total fluid pressures, assuming gas magma saturation, were assessed from the few available values of CO_2 and H_2O in primitive MI. The pressures ($P_{CO_2} + P_{H_2O}$) were computed between 240 and 300 MPa (Table 2), using VolatileCalc [*Newman and Lowernstern*, 2002], and for a basalt containing 48 wt % SiO_2, as deduced from the coefficient [*Dixon*, 1997]. Using *Papale*'s [1999] model, they shift to higher values up to 400 MPa. The effect of water on the CO_2 solubility in basaltic melts at high pressure [*Botcharnikov et al.*, 2005] also limits the application of the available models. It is worth noting, however, that the 5 April 2003 samples plot in the pressure domain defined from the olivine-hosted MI of the large-scale historical paroxysms [*Métrich et al.*, 2001; *Bertagnini et al.*, 2003].

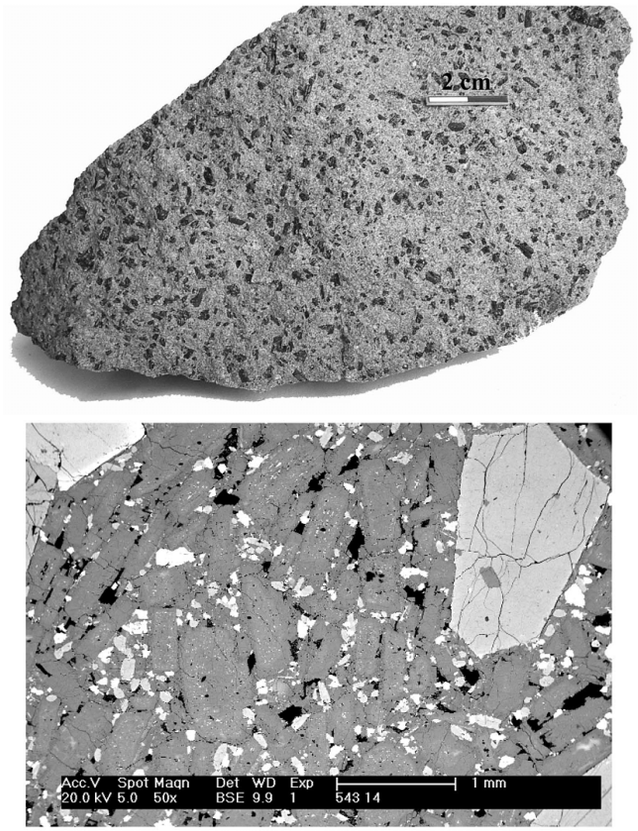

Figure 8. Macroscopic and microscopic (SEM) features of the 5 April 2003 subvolcanic igneous ejecta [type 1: *Pistolesi et al.*, this volume].

3. SUBVOLCANIC LITHIC EJECTA

3.1. Petrography and Mineral Chemistry of the Lithic Ejecta

Subvolcanic igneous blocks consist of gray holocrystalline rocks (type 1; Figure 8), locally brecciated and more or less welded by a dark gray vesicle-rich lava-like or scoria lithotype (types 2 and 3 ejecta, respectively; *Pistolesi et al.*, this volume; *Renzulli et al.*, 2008). They are phaneritic with phenocrysts of plagioclase (~28 vol %), clinopyroxene (~15 vol %), and olivine (~5 vol %). Interstitial crystallization of thinner-grained plagioclase, sanidine, clinopyroxene, olivine, opaque minerals (Ti-magnetite and ilmenite), apatite, and phlogopite also occurs (Figure 8). Sanidine is usually present in the finer-grained interstitial component as anhedral-poikilitic phase and as rims overgrowth, up to 50 μm thick, on plagioclase phenocrysts (Figure 8). At the microscale, igneous lamination is ubiquitous, involving plagioclase phenocrysts and microphenocrysts showing a clear preferred orientation. When the subvolcanic blocks are brecciated and welded (type 2), the closely associated dark gray vesicle-rich lava-like component [*Pistolesi et al.*, this volume] is porphyritic, with about 50 vol % of olivine, clinopyroxene, and plagioclase phenocrysts whose grain size resembles those of the gray igneous lithotype (Figure 8). Its groundmass is microcrystalline to cryptocrystalline, made of abundant sanidine, plagioclase, clinopyroxene, opaque minerals, and rare pigeonite and olivine. Sanidine is commonly interstitial, but it also occurs as rare, thin overgrowths on plagioclase. Contacts between the two components of the subvolcanic welded breccias usually show brittle features with broken crystals of the gray subvolcanic igneous block. Enrichment of vesicles in the dark gray rock often occurs close to the contact zone [*Pistolesi et al.*, this volume].

Texture and composition of inner plagioclase, olivine, and clinopyroxene phenocrysts from subvolcanic igneous blocks are closely similar to those of the same minerals from crystal-rich scoriae and lavas of the present-day Stromboli activity [*Métrich et al.*, 2001; *Francalanci et al.*, 2004b; *Landi et al.*, 2004, 2006; *Bertagnini et al.*, this volume] (Figures 9 and 10). Conversely, the composition is more evolved towards the rims and in the interstitial grains of the groundmass, up to plagioclase An_{25}, olivine Fo_{50}, and augite $Wo_{5–9}$–$En_{61–62}$–$Fs_{30–33}$ (Figures 9 and 10). Alkali feldspar, occurring as plagioclase rims and anhedral-poikilitic phase, shows a Na-sanidine composition ($Or_{49–56}$–$Ab_{40–44}$–$An_{4–7}$) and high BaO contents (up to 4.2 wt %).

In addition, Mg-pigeonite microlites are found in the dark gray vesicle-rich component of the welded breccias. The presence of pigeonite could be explained by the expansion of the pigeonite stability field with the increasing differentia-

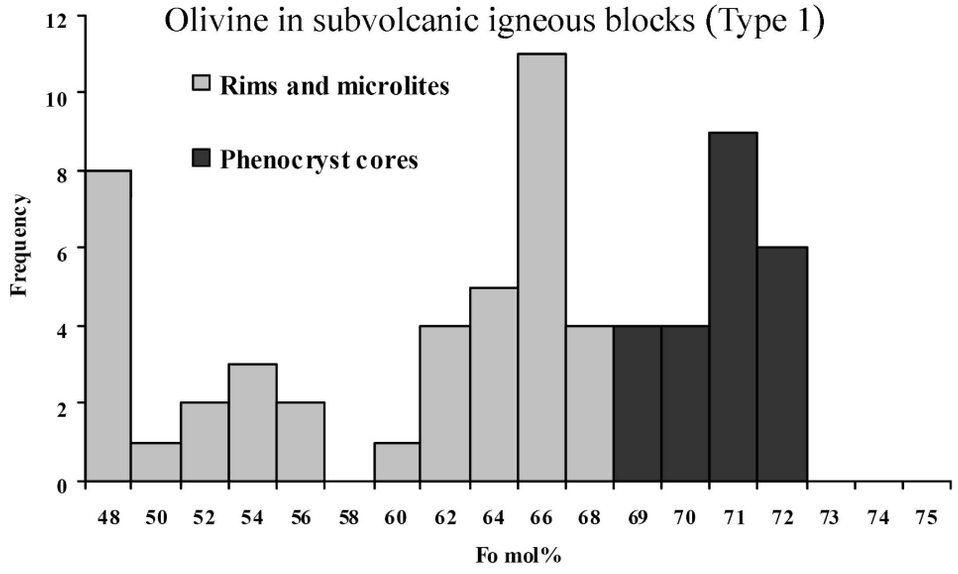

Figure 9. Olivine composition in the most common subvolcanic lithotype ejecta (type 1). It is worth noting that olivine phenocryst cores have the same composition of the phenocrysts and microphenocrysts of the high porphyritic scoriae and lavas, whereas olivine rims and microlites of the subvolcanic lithotype are significantly enriched in iron.

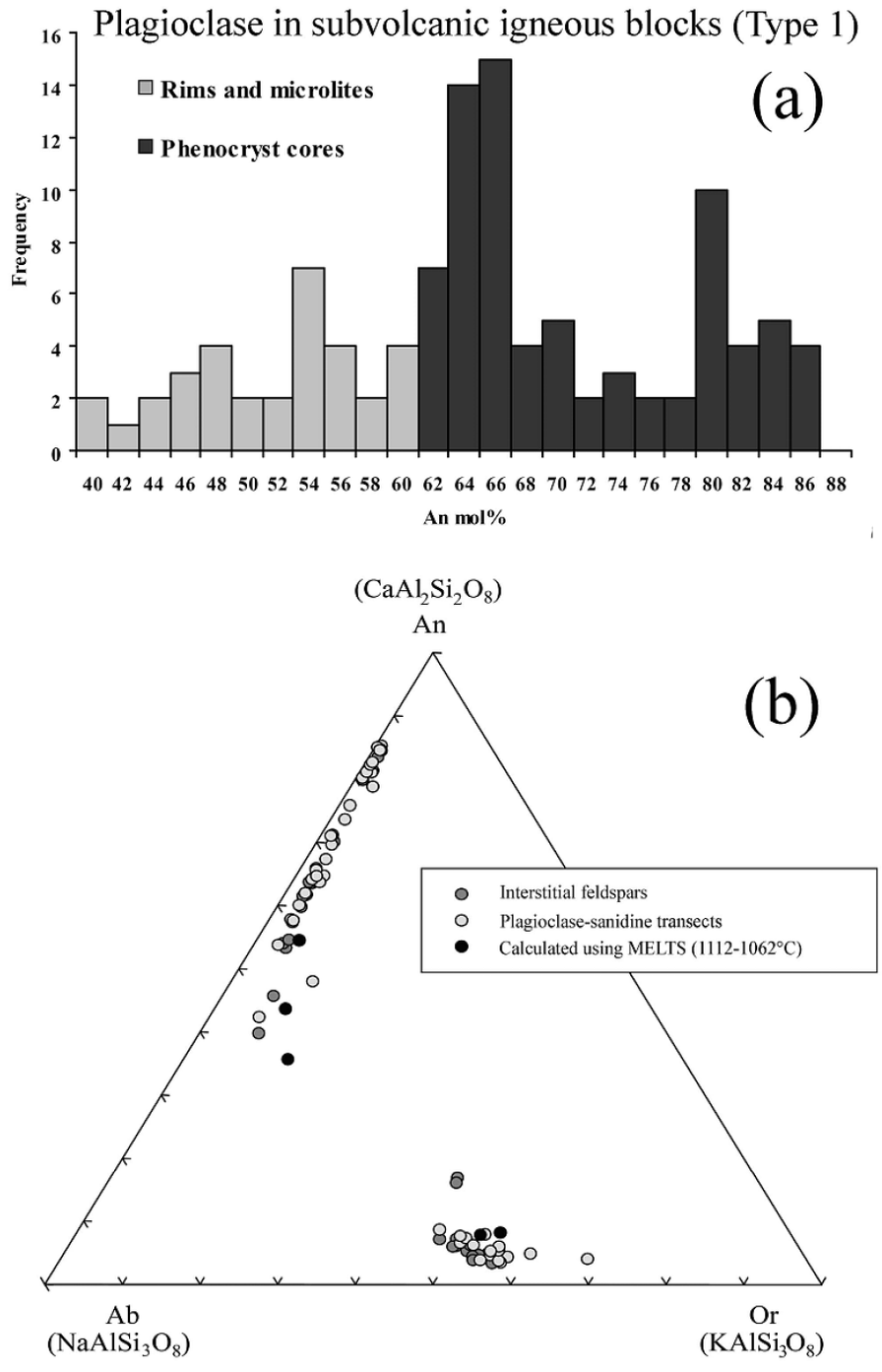

Figure 10. (a) Plagioclase composition in the most common subvolcanic lithotype ejecta [type 1: *Pistolesi et al.*, this volume]. It is worth noting that plagioclase phenocryst cores have the same composition of the phenocrysts and microphenocrysts of the high porphyritic scoriae and lavas, whereas plagioclase rims and microlites of the subvolcanic lithotypes are significantly enriched in the Ab molecule. (b) Feldspar ternary diagrams for the subvolcanic type 1 ejecta.

tion degree and iron enrichment of the residual melt. Expansion of the pigeonite stability field appears to be a transient phenomenon [*Renzulli et al.*, 2008].

Opaque minerals are represented by both Ti-magnetite and ilmenite. Equilibrium temperatures of these oxide pairs range between 790° and 830°C using the geothermometers of *Powell and Powell* [1977] and *Spencer and Lindslay* [1981]. These temperatures are between the HM and NNO buffers, indicating a log fO_2 ranging from −13.8 to −12.9. Since the opaque mineral pairs represent the late-stage magmatic crystallization, the above temperature values are supposed to approach the solidus curve of the shoshonitic basalts which formed the shallow-level subvolcanic body. It is worth noting that ilmenite is not found throughout the shoshonitic basalts (scoria or lavas) of the present-day activity. This is because the porphyritic basalts are normally erupted at temperature of ~1090°C [*Freda et al.*, 2005], well above the ilmenite liquidus. Ilmenite may, therefore, crystallize when some residual liquids become enriched in TiO_2 and temperature is low enough to equilibrate oxide pairs [*Renzulli et al.*, 2008].

3.2. Whole-Rock Geochemistry and Glass Composition of the Lithic Ejecta

The subvolcanic igneous blocks are shoshonitic basalts, with major and trace element compositions similar to the crystal-rich scoria and lavas (Figure 4), suggesting these blocks could simply represent small batches of crystal-rich magma arrested in the uppermost plumbing system of the present-day activity [*Renzulli et al.*, 2004, 2008]. In the breccias, both the gray vesicle-free and the dark gray vesicle-rich rocks have comparable major and trace element contents (Table 4).

Sr isotope ratios of the subvolcanic blocks show small variation, ranging from 0.706151 to 0.706175. Both Sr and Nd isotope ratios of the studied lithics have values similar to those of the products from the most recent Strombolian activity (Table 3; Figure 4). Indeed, Sr isotope ratios generally decrease with time after 1985, starting from a value of about 0.70626 [*Francalanci et al.*, 1999]. Accordingly, the $^{87}Sr/^{86}Sr$ values of subvolcanic blocks akin to those of the scoria and lavas erupted during the last 10 years (Figure 4). This is also in agreement with the freshness of these lithics [*Francalanci et al.*, 2003].

Rare glassy mesostasis of trachyte composition were detected (by scanning electron microscopy with energy dispersive spectrophotometer analyses) in the subvolcanic blocks of 5 April 2003. In addition, according to mass balance calculations, the composition resulting from bulk rock of the subvolcanic ejecta minus their "phenocrystic" components (i.e., the coarser-grained crystals) closely matches that of the glassy groundmass of the erupted crystal-rich basalts of the present-day activity. This means that the silicate liquid normally frozen as glass in the crystal-rich lavas and scoria is the same from which the interstitial, finer-grained mineral assemblage of the subvolcanic blocks is crystallized. According to MELTS code (Melts-Linux-RH-ELF 3.0.5; *Ghiorso and Sack*, 1995; *Asimow and Ghiorso*, 1998), the melt otherwise quenched as glass in the extrusives may produce a liquid line of descent that passes through the residual glassy mesostasis of the subvolcanic blocks. MELTS calculations were investigated within the quartz–fayalite–magnetite buffer, at temperatures lower than the eruption temperatures of the crystal-rich basaltic magma and considering a pressure of 0.5 kbar. This pressure value is compatible with the stationary level of the crystal-rich basaltic magma of Stromboli being considered within the volcanic cone by geophysical and petrological evidences. Along this liquid line of descent, the mineralogy (olivine, $Fo_{56–60}$; clinopyroxene, $En_{37–44}$, $Fs_{13–17}$, $Wo_{41–42}$; plagioclase, $Ab_{43–51}$, $An_{36–50}$, $Or_{7–13}$; sanidine, $Or_{51–55}$, $An_{4–8}$, $Ab_{37–45}$) obtained by MELTS calculations is similar to that of the finer-grained minerals of the type 1 subvolcanic blocks. The crystallization of the finer-grained phases of type 1 blocks are therefore normally precluded in the present-day crystal-rich basalts because of the high degree of undercooling of the erupted magmas [*Renzulli et al.*, 2008].

4. CONCLUSIONS

Available chemical information on whole rocks, matrix glasses, and minerals shows that pumices and scoria erupted by the 5 April paroxysm generally have textural, mineralogical, major and trace elements, and isotopic characteristics similar to those of their analogs erupted by the earlier paroxysms. Nevertheless, some significant differences have been recognized: (1) the 5 April 2003 pumices do not carry Mg-rich olivines (Fo~90) with Ca-rich primitive MI that testify to magma input in the deep-feeding system as recognized for the large-scale paroxysms [*Bertagnini et al.*, this volume]; (2) the olivine + clinopyroxene mineral assemblage, usually observed in equilibrium with the crystal-poor magma erupted as pumice, is rarely found; (3) the bulk-rock and glassy matrix chemistry of 5 April 2003 pumice is characterized by lower Cr and Sc contents than previously erupted pumices.

Both the mineralogy of the 5 April 2003 pumice and the chemistry of the olivine-hosted MI imply that the gas/particle jets were driven by the fragmentation of a volatile-rich, strongly mixed and mingled magma batch. Most of the crystals show resorption features to variable extents that prove their entrainment from the more evolved parts of the plumb-

Table 4. Major and Trace Element Data of Subvolcanic Lithic Blocks

	STR[a] 050403r	STR[b] 050403r	STR[a] 050403s	STR[b] 050403s	STR[a] 050403t	STR[a] 050403y	STR[b] 050403y	5437a1[c]	5437a2/v[c]	5437f/v[c]	5437g1[c]	5437g2/v[c]	54314/Sc[c]	54314/Ch[c]
SiO_2	50.98	50.27	50.58	49.96	50.70	50.91	50.11	50.10	49.55	49.79	50.00	49.44	49.47	49.64
TiO_2	0.82	0.94	0.88	0.93	0.83	0.78	0.94	0.95	0.91	0.92	0.94	0.90	0.94	0.94
Al_2O_3	18.78	17.44	17.95	17.29	18.62	18.69	17.39	17.01	16.67	16.42	16.84	16.48	17.22	17.04
Fe_2O_3	1.16	8.89	3.06	8.86	1.59	1.28	8.90	8.80	8.76	8.81	8.84	8.83	8.69	8.84
FeO	6.10	–	4.82	–	5.81	5.73	–	–	–	–	–	–	–	–
MnO	0.14	0.16	0.15	0.16	0.15	0.14	0.16	0.16	0.16	0.16	0.16	0.16	0.15	0.15
MgO	6.33	6.12	6.64	6.11	6.12	6.84	6.09	6.07	6.41	6.56	6.23	6.50	5.88	6.10
CaO	10.35	11.11	10.56	11.19	10.52	10.24	11.17	11.09	11.17	11.52	11.19	11.28	11.18	11.12
Na_2O	2.53	2.52	2.55	2.51	2.65	2.55	2.47	2.52	2.56	2.51	2.54	2.59	2.59	2.60
K_2O	2.20	2.15	2.20	2.15	2.45	2.27	2.11	2.28	2.25	2.27	2.29	2.28	2.17	2.21
P_2O_5	0.50	0.55	0.43	0.56	0.49	0.52	0.55	0.55	0.53	0.51	0.54	0.52	0.55	0.55
LOI	0.09	0.01	0.18	0.01	0.08	0.07	0.01	–	–	–	–	–	–	–
Tot	99.98	100.14	100.00	99.71	100.01	100.02	99.89	99.15	98.80	99.25	99.20	98.84	98.53	98.76
V	231	252	252	256	230	226	255	236	240	231	226	226	226	223
Cr	50	38	49	45	54	49	43	54	59	67	57	59	35	41
Co	29	32.1	31	33.5	29	29	31.8	29	29	28	27	28	27	28
Ni	–	35	–	36	–	–	36	52	41	43	38	40	37	38
Sc	–	29	–	29	–	–	30	–	–	–	–	–	–	–
Cu	89	102	93	109	109	103	114	132	57	53	125	49	96	68
Zn	56	65	62	65	56	55	65	87	91	83	80	82	84	81
Ga	–		–	–	–	–	–	16	16	15	16	15	16	16
Cs	–	4.0	–	5.0	–	–	3.8	6.3	4.0	4.6	4.7	3.2	4.6	3.2
Rb	61	68	61	72	69	60	69	74	69	69	71	66	70	69
Sr	778	735	787	750	812	776	749	836	840	794	775	796	843	833
Y	25	25.9	26	27.7	26	25	27.4	28	28	27	27	27	27	28
Zr	141	140	149	143	151	142	142	175	170	158	158	163	158	164
Nb	19	20.6	21	21.4	22	20	21.5	20	20	20	21	20	21	22
Ba	1055	930	1013	932	1149	1060	928	1100	1090	1040	1100	1050	1060	1070
La	46.5	44.0	51.8	47.4	51.6	46.9	45.6	52.5	50.6	51.2	51.9	52.8	50.2	49.5
Ce	95.3	95.8	100.2	104.1	97.0	103.2	100.6	103.9	98.5	100.0	102.8	103.4	101.0	98.0
Pr	–	11.3	–	12.4	–	–	12.1	10.6	10.1	10.3	10.5	10.6	10.3	10.1
Nd	44.9	42.8	48.5	46.9	43.3	48.8	44.7	43.2	41.8	43.2	43.0	43.8	41.8	41.5
Sm	–	8.4	–	9.1	–	–	8.7	8.7	8.4	8.7	8.7	8.8	8.6	8.3
Eu	–	2.3	–	2.5	–	–	2.3	2.3	2.2	2.3	2.2	2.3	2.3	2.2
Gd	–	7.0	–	7.7	–	–	7.3	7.5	7.2	7.5	7.3	7.6	7.3	7.4
Tb	–	1.1	–	1.1	–	–	1.1	1.1	1.0	1.1	1.0	1.1	1.1	1.0
Dy	–	5.2	–	5.7	–	–	5.4	5.3	5.1	5.3	5.3	5.2	5.2	5.1
Ho	–	1.0	–	1.1	–	–	1.0	1.0	0.9	0.9	0.9	0.9	0.9	0.9
Er	–	2.6	–	2.8	–	–	2.7	2.8	2.7	2.8	2.7	2.8	2.7	2.7
Tm	–	0.35	–	0.37	–	–	0.37	0.37	0.37	0.38	0.37	0.39	0.38	0.38
Yb	–	2.4	–	2.6	–	–	2.5	2.4	2.2	2.3	2.4	2.3	2.3	2.3
Lu	–	0.36	–	0.39	–	–	0.38	0.36	0.35	0.37	0.36	0.34	0.36	0.36
Ta	–	1.4	–	1.5	–	–	1.4	1.1	1.1	1.1	1.1	1.1	1.0	1.1
Hf	–	3.7	–	3.8	–	–	3.8	4.3	4.2	4.2	4.0	4.4	4.0	4.2
Pb	16	18	17	17	15	13	17	15	16	14	13	17	15	12
Th	–	15.1	–	16.1	–	–	15.4	16.1	15.2	15.7	15.6	16.1	15.6	15.4
U	–	3.72	–	3.97	–	–	3.76	4.14	3.99	4.08	4.04	4.25	4.09	4.06

[a] All the elements were analyzed by XRF at the Department of Earth Science of Florence, Italy.

[b] Major elements were analyzed by XRF and trace elements by ICP–atomic emission spectrometry + ICP–MS at the SGS Minerals Services of Toronto, Canada.

[c] Major elements were analyzed by ICP–optical emission spectroscopy and trace elements by ICP–MS at the Actlabs Laboratory, Ontario, Canada.

ing system. Furthermore, the Sr isotope disequilibria between groundmass and minerals suggest that the inner parts of the zoned crystals are xenocrysts derived from a cumulus crystal-mush zone. These xenocrysts crystallized from previous magmas (>1900 A.D.), when the volcanic products were more Sr-radiogenic than those erupted at present. Noticeably, Sr isotope disequilibrium is also found between outer rims and groundmass of crystals from the 2003 post-paroxysm lavas; this provides evidence that the uprise of crystal-poor magmas brought new xenocrysts in the shallow magmatic system [*Landi et al.*, this volume; Nardini et al., submitted manuscript, 2008].

A few olivine crystals ($Fo_{85–87}$) record the involvement of a more primitive melt with a total dissolved volatile content of 3.1 wt % (H_2O, CO_2, S, Cl), which allows estimating a total fluid pressure ≥240 MPa. The involvement of a more primitive melt relative to that poured out as pumice is testified by olivine hosted MI; however, its imprint on the composition of the erupted magma is weak. This is a recurrent characteristic of the Stromboli paroxysms and strongly indicates that the "deep" magma blobs—uprising from depths corresponding to 200–300 MPa P conditions—have small volumes. In turn, this implies that the driving force for triggering magma ascent is chiefly supplied by gas bubbles. The high volume ratio between gas and melt is testified by the heterogeneous trapping of gas and melt within crystals [*Métrich et al.*, 2005], with possible gas differential transfer from a bubble-rich layer where gas bubbles accumulated and coalesced in the range of pressure reported above [*Allard*, 2004].

The slightly lower contents of compatible trace elements of 5 April pumice, relative to that of older pumices, suggest that the 5 April crystal-poor magmas fractionated a higher amount of femic phases (mainly clinopyroxene).

En route to the surface, the gas-rich and crystal-poor magma blob interacts and mixes with overlying melts, filling the feeding system of the volcano [*Bertagnini et al.*, 2003]. It also continues to exsolve volatiles that promote bubble growth and expansion. Following this line of reasoning, the crystal-poor magma that erupted by the 5 April paroxysm most likely represents the upper part of the deep plumbing system that is still able to generate pumice. In the final stage, immediately before magma fragmentation and explosion, this "balloon" of vesicular magma rapidly rises through and mingles with the denser, degassed magma residing in the uppermost part of the cone.

The subvolcanic blocks ejected during the 5 April 2003 paroxysm have the same uniform chemical and isotopic composition, which characterizes the crystal-rich products erupted during the present-day explosive and effusive activity of the volcano. Microstructures and chemistry of crystals larger than 100–150 m closely match those of the phenocrysts and microphenocrysts of the crystal-rich scoriae and lavas. ~~Control Strategy Development~~ data [*Renzulli et al.*, 2008] give a residence time for the finer-grained interstitial olivine of about 100 d, assuming a crystal growth value for olivine of 10^{-8} mm/s [*Armienti et al.*, 1994]. As a result, finer-grained mineral assemblage (finer than 100 m) could be crystallized during brief periods in which small batches of crystal-rich magma arrest and crystallize in the uppermost part of the subvolcanic system. The ~~cause of the~~ complete solidification of the present-day crystal-rich basaltic magma ~~might be ascribed to~~ the drainage of magma from the surface to lower levels~~, which occurred at the beginning of the effusive event, and its crystallization during~~ the short break of the summit explosive activity in the period 28 December 2002–early March 2003 [*Cortés et al.*, 2006; *Renzulli et al.*, 2008].

Acknowledgments. We would like to thank Maurizio Ulivi, Elena Boari, and Massimo Tiepolo for laboratory assistance. Riccardo Petrini is acknowledged for the critical revision of the manuscript. This research was financially supported by INGV and Italian Civil Defence (DPC).

REFERENCES

Allard, P. (2004), Stromboli, an erupting system powered by steady and catastrophic gas transfer. INGV Workshop: L'eruzione di Stromboli (28 Dicembre 2002–20 Luglio 2003), 21–24 May 2004, Catania, Italy, Abstract, p. 7.

Anders, E., and N. Grevesse (1989), Abundances of the elements: Meteoric and solar, *Geochim. Cosmochim. Acta*, *53*, 197–214.

Armienti, P., M. T. Pareschi, F. Innocenti, and M. Pompilio (1994), Effects of magma storage and ascent on the kinetics of crystal growth. The case of 1991–93 Mt. Etna eruption, *Contrib. Mineral. Petrol.*, *115*, 402–414.

Asimow, P. D., and M. S. Ghiorso (1998), Algorithmic modifications extending MELTS to calculate subsolidus phase relations, *Am. Mineral.*, *83*, 1127–1132.

Avanzinelli, R., E. Boari, S. Conticelli, L. Francalanci, L. Guarnieri, G. Perini, C. M. Petrone, S. Tommasini, and M. Ulivi (2005), High precision Sr, Nd, and Pb isotopic analyses using new generation Thermal Ionisation Mass Spectrometer ThermoFinnigan Triton-Ti®, *Period. Mineral.*, *74–73*, 147–166.

Barberi, F., M. Rosi, and A. Sodi (1993), Volcanic hazard assessment at Stromboli based on review of historical data, *Acta Vulcanol.*, *3*, 173–187.

Bertagnini, A., N. Métrich, P. Landi, and M. Rosi (2003), Stromboli volcano (Aeolian Archipelago, Italy): An open window on the deep-feeding system of a steady state basaltic volcano, *J. Geophys. Res.*, *108*(B7), 2336, doi:10.1029/2002JB002146.

Botcharnikov, R., M. Freise, F. Holtz, and H. Berhens (2005), Solubility of C–O–H mixtures in natural melts: New experimental data and application range of recent models, *Ann. Geophys.*, in press.

Dixon, J. B. (1997), Degassing of alkalic basalts, *Am. Mineral.*, *82*, 368–378.

Charlier, B. L. A., C. Ginibre, D. Morgan, G. M. Nowell, D. G. Pearson, J. P. Davidson, and C. J. Ottley (2006), Methods for the microsampling and high-precision analysis of strontium and rubidium isotopes at single crystal scale for petrological and geochronological applications, *Chem. Geol.*, *232*, 114–133.

Cortés, J. A., M. Wilson, E. Condliffe, and L. Francalanci (2006), The occurrence of forsterite and highly oxidizing conditions in basaltic lavas from Stromboli volcano, Italy, *J. Petrol.*, *47*, 1345–1373.

Francalanci, L., P. Manetti, and A. Peccerillo (1989), Volcanological and magmatological evolution of Stromboli volcano (Aeolian islands): The roles of fractional crystallisation, magma mixing, crustal contamination and source heterogeneity, *Bull. Volcanol., 51*, 355–378.

Francalanci, L., S. Tommasini, S. Conticelli, and G. R. Davies (1999), Sr isotope evidence for short magma residence time for the 20th century activity at Stromboli volcano, Italy, *Earth Planet. Sci. Lett.*, *167*, 61–69.

Francalanci, L., M. Rosi, S. Tommasini, S. Conticelli, E. Germiniani, C. Petrone, A. Bertagnini, P. Landi, and R. Vannucci (2003), Caratteristiche mineralogiche, geochimiche ed isotopiche dei prodotti emessi durante l'attuale crisi eruttiva di Stromboli: Implicazioni sui meccanismi pre-eruttivi del sistema vulcanico. GNV-INGV, General Assembly, Roma, Giugno, Abstracts, 30–31.

Francalanci, L., I. Nardini, D. G. Chertkoff, S. Conticelli, and J. P. Davidson (2004a), The pre-eruptive processes involved in the 2002–2003 crisis at Stromboli volcano, Italy: Inferences from detailed mineralogical, geochemical and isotopic data on the erupted products. Italia 2004, 32° International Geological Congress, Firenze, Agosto, Abstracts, Part 2, 207–205, p. 967.

Francalanci, L., S. Tommasini, and S. Conticelli (2004b), The volcanic activity of Stromboli in the 1906–1998 AD period: Mineralogical, geochemical and isotope data relevant to understanding of the plumbing system, *J. Volcanol. Geotherm. Res.*, *131*, 179–211.

Francalanci, L., G. R. Davies, W. Lustenmhower, S. Tommasini, P. R. D. Mason, and S., Conticelli, (2005), Old crystal re-cycle and multiple magma reservoirs in the plumbing system of the present day activity at Stromboli volcano, South Italy: Sr-isotope in situ microanalyses, *J. Petrol*., *46*, 1997–2021, doi:10.1093/petrology/egi045.

Freda, C., D. R. Baker, and P. Scarlato (2005), Sulfur diffusion in basaltic melts, *Geochim. Cosmochim. Acta*, *69*, 5061–5069.

Ghiorso, M. S., and R. O. Sack (1995), Chemical mass transfer in magmatic processes; IV, A revised and internally consistent thermodynamic model for the interpolation and extrapolation of liquid–solid equilibria in magmatic systems at elevated temperatures and pressures, *Contrib. Mineral. Petrol.*, *119*, 197–212.

Landi, P., N. Métrich, A. Bertagnini, and M. Rosi (2004), Dynamics of magma mixing and degassing in plagioclase at Stromboli (Aeolian Archipelago, Italy), *Contrib. Mineral. Petrol.*, *147*, 213–227.

Landi, P., L. Francalanci, M. Pompilio, M. Rosi, R. A. Corsaro, C. M. Petrone, I. Nardini, and L. Miraglia (2006), The December 2002–July 2003 effusive event at Stromboli volcano, Italy: Insights into the shallow plumbing system by petrochemical studies, *J. Volcanol. Geotherm. Res.*, *155*, 263–284.

Landi, P., L. Francalanci, R. A. Corsaro, C. M. Petrone, A. Fornaciai, M. Carroll, I. Nardini, and L. Miraglia (this volume), Textural and compositional characteristics of the lavas erupted in the December 2002–July 2003 effusive events at Stromboli, Aeolian Island, Italy.

Latypov, R. M., M. I. Dubrovskii, and T. T. Alapieti (2001), Graphical analysis of the orthopyroxene–pigeonite–augite–plagioclase equilibrium at liquidus temperatures and low pressure, *Am. Mineral.*, *86*, 547–554.

Métrich, N., A. Bertagnini, P. Landi, and M. Rosi (2001), Crystallisation driven by decompression and water loss at Stromboli volcano (Aeolian Islands), *J. Petrol.*, *42*, 1471–1490.

Métrich, N., A. Bertagnini, P. Landi, M. Rosi, and O. Belhadj (2005), Triggering mechanism at the origin of paroxysms at Stromboli (Aeolian archipelago, Italy): The 5 April 2003 eruption, *Geophys. Res. Lett.*, *32*, L103056, doi:10.1029/2004GL022257.

Newman, S., and J. B. Lowernstern (2002), VolatileCalc: A silicate melt–H_2O–CO_2 solution model written in Visual Basic Excel, *Comput. Geosci.*, *28*, 597–604.

Papale, P. (1999), Modeling of the solubility of two-component H_2O–CO_2 fluid in silicate liquids, *Am. Mineral.*, *84*, 477–492.

Pistolesi, M., M. Rosi, L. Pioli, A. Renzulli, A. Bertagnini, and D. Andronico (this volume), The paroxysmal explosion and its deposits.

Powell, M., and R. Powell (1977), Geothermometry and oxygen barometry using coexisting iron titanium oxides: A reappraisal, *Mineral. Mag.*, *41*, 257–263.

Renzulli, A., P. Landi, A. Bertagnini, M. Rosi, M. Menna, and S. Del Moro (2004), Subvolcanic crystallization of the present-day shoshonitic basalts of Stromboli: Evidence from the ejecta erupted on April 5th 2003. Incontro Scientifico dell'INGV "L'eruzione di Stromboli (28 Dicembre 2002–20 Luglio 2003)," 20–21 Maggio 2004, Catania.

Renzulli, A., S. Del Moro, M. Menna, P. Landi, and M. Piermattei (in press), Transient processes in the shallow basaltic system of Stromboli (Aeolian Islands, Italy) inferred from dolerites and magmatic breccias erupted as blocks during the paroxysm of 5 April 2003, *Bull. Volcanol*. Q5

Rosi, M., A. Bertagnini, A. J. L. Harris, L. Pioli, M. Pistolesi, and M. Ripepe (2006), A case history of paroxysmal explosion at Stromboli: Timing and dynamics of the April 5, 2003 event, *Earth Planet. Sci. Lett.*, *243*(3–4), 594–606.

Spencer, K. J., and D. H. Lindsley (1981), A solution model for coexisting iron–titanium oxides. *Am. Mineral.*, *66*, 1189–1201.

Tiepolo, M., P. Bottazzi, M. Palenzona, and R. Vannucci (2003), A laser probe coupled with ICP—Double-focusing sector-field mass spectrometer for in situ analysis of geological samples and U–Pb dating of zircon, *Can. Mineral.*, *41*, 259–272.

Thirlwall, M. F. (1991), Long-term reproducibility of multicollector Sr and Nd ratio analyses, *Chem. Geol.*, *94*, 85–104.

Tommasini, S., A. Heumann, R. Avanzinelli, and L. Francalanci (2007), The fate of high angle dipping slabs in the subduction factory: An integrated trace element and radiogenic isotope (U, Th, Sr, Nd, Pb) study of the Stromboli volcano, Aeolian arc, Italy, *J. Petrol.*, *48*(12), 2407–2430.

A. Bertagnini and P. Landi, Istituto Nazionale di Geofisica e Vulcanologia, Sezione di Pisa, Via della Faggiola 32, 56126 Pisa, Italy.

S. Del Moro, M. Menna, and A. Renzulli, Istituto di Scienze della Terra, Università degli Studi di Urbino, Campus Scientifico, 61029, Urbino, Italy.

L. Francalanci, I. Nardini, and C. M. Petrone, Dipartimento di Scienze della Terra, Università degli Studi di Firenze, via La Pira 4, 50121, Firenze, Italy. (lorella.francalanci@unifi.it)

N. Métrich, Laboratoire Pierre Süe, CEA-CNRS, CE-Saclay, 91191 Gif-sur-Yvette, France.

R. Vannucci, Dipartimento di Scienze della Terra, Università di Pavia, e CNR-IGG, via Ferrata 1, 27100 Pavia, Italy.

Author Query Form

(Queries are to be answered by the Author)

Chapter 18 – AGU Calvari

The following queries have arisen during the typesetting of your manuscript. Please answer these queries.

Query Marker	Query	Reply
Q1	"...although our efforts for separating the two fractions." was changed to "...despite our efforts in separating the two fractions." Please check if appropriate.	
Q2	≤Fo71: "71" was set in subscript. Please check if appropriate. OK?	
Q3	Please advise if "100–150 m" and "(finer than 100 m)" should be retained as is; that is, if they should be in meters.	
Q4	Please provide update on the publication status of "Botcharnikov et al. 2005 (in press)."	
Q5	Please provide update on the publication status of "Renzulli et al. 2008 (in press)."	

Thank you very much.